Serbian Journal of Geosciences **11 (2025)**
University of Niš, Faculty of Sciences and Mathematics

Detection and mapping of gullies in forested terrain using UAV LiDAR-derived DEMs

Milan Đorđević[1], **Miloš Manić**[2]

[1]Faculty of Sciences and Mathematics, Department of Geography, Višegradska 33, Niš, Serbia
[2]Faculty of Geography, Studentski trg 3, Belgrade, Serbia

Received 12. 02. 2026 · Accepted for publication 15. 02. 2026

Keywords:

UAV LiDAR,
gully erosion,
topographic openness,
forested terrain,
digital elevation model,
remote sensing.

Abstract

Accurate detection of gullies and delineation of their boundaries in forested terrain remain significant challenges for erosion monitoring and land management. Traditional remote sensing methods, including satellite imagery and aerial photogrammetry, are often ineffective beneath dense vegetation canopy. This study presents a semi-automated methodology for gully boundary delineation using high-resolution UAV LiDAR data combined with topographic openness analysis. The research was conducted in the Crveni Potok catchment near Niš, Serbia, a forested catchment of approximately 8 km² where large gullies hidden under forest canopy were discovered during initial field surveys. The methodology comprises UAV LiDAR data acquisition and processing, point cloud classification, generation of a 10 cm resolution digital elevation model, computation of positive topographic openness, reclassification and vectorization of gully zones, and validation against previously documented gullies from terrestrial photogrammetric studies. Results demonstrate that UAV LiDAR successfully penetrates dense vegetation, enabling reliable detection of gullies invisible in conventional satellite imagery. This semi-automated approach provides accurate and efficient gully mapping, improving erosion monitoring capabilities in forested catchments and offering significant implications for soil conservation planning in similar terrain conditions.

1. Introduction

Gully erosion, characterized by the formation of deeply incised channels, is particularly severe as it can rapidly remove large volumes of soil and sediment (Poesen et al., 2003; Valentin et al., 2005). Understanding the spatial distribution and morphology of gullies is essential for effective erosion control and watershed management.

Traditional methods for mapping gullies rely heavily on field surveys and conventional remote sensing techniques. However, field surveys are time-consuming, labor-intensive, and often limited in spatial coverage. Satellite imagery and aerial photography, while providing broader coverage, face significant limitations in forested areas where dense vegetation obscures ground features (Kropáček et al., 2016). These challenges are particularly acute in mixed-use watersheds where gullies may develop under forest canopy, remaining undetected until they cause substantial environmental damage.

Recent advances in Light Detection and Ranging (LiDAR) technology, particularly Unmanned Aerial Vehicle (UAV)-mounted systems, offer new opportunities for terrain characterization beneath vegetation cover (Vosselman and Maas, 2010; Jaboyedoff et al., 2012). Unlike passive optical sensors, LiDAR actively emits laser pulses that can penetrate gaps in vegetation canopy and record multiple returns, enabling the reconstruction of bare-earth terrain even under dense forest cover (Hodgson and Bresnahan, 2004; Liu, 2008).

Corresponding author. e-mail address: milan.djordjevic@pmf.edu.rs (Đorđević M.)
https://doi.org/10.18485/srbjgeosci.2025.11.1.4

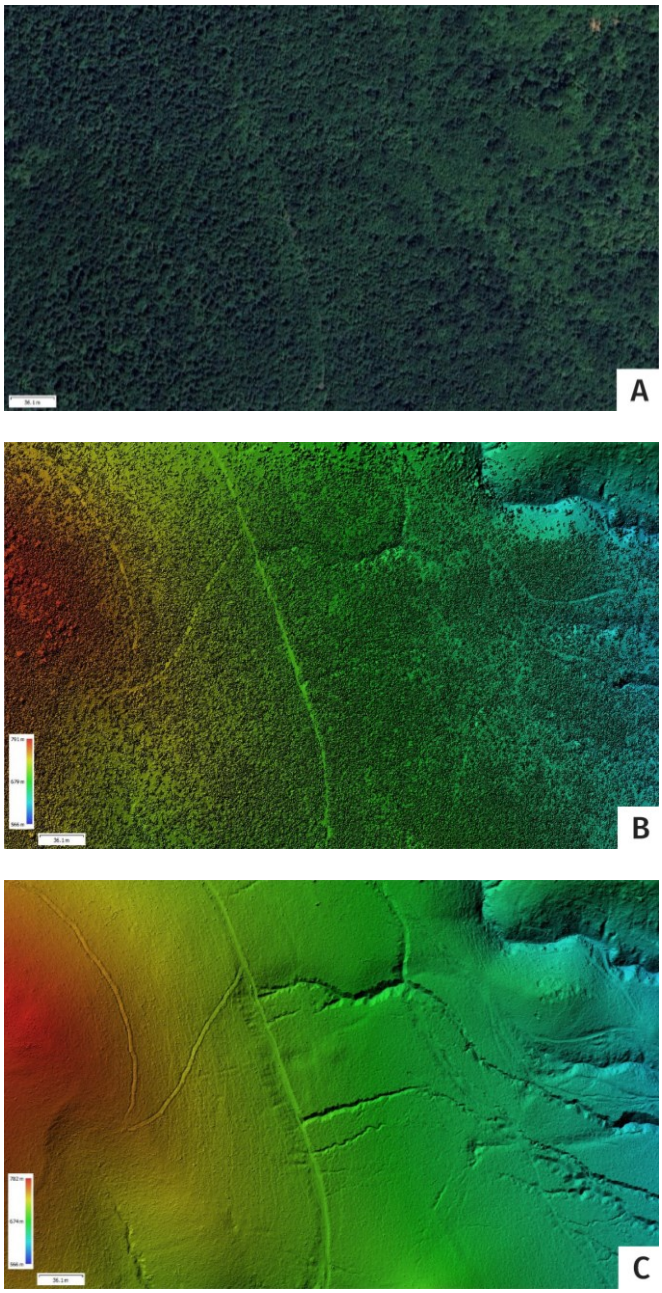

Figure 1. *Comparison of data sources for the study area: (A) conventional satellite/aerial optical imagery showing dense forest canopy with no visible terrain features; (B) UAV LiDAR point cloud with vegetation returns, color-coded by elevation; (C) bare-earth DEM derived from classified ground points, revealing gully networks hidden beneath the canopy.*

Topographic indices derived from high-resolution DEMs have proven effective for identifying geomorphological features. Among these, topographic openness—a measure of terrain convexity and concavity—has shown particular promise for detecting gully systems (Yokoyama et al., 2002; Doneus, 2013; Challis, 2006). Positive openness highlights concave features such as valleys and gullies, making it well-suited for automated feature extraction. Recent studies have also employed various DEM-based methods for gully detection, including slope-area analysis (Walker et al., 2024), curvature-based approaches (Na et al., 2018), and hydrological modeling techniques (Zhao et al., 2023).

This study presents a semi-automated methodology for extracting gully boundaries in forested terrain using high-resolution UAV LiDAR data. The research was motivated by the unexpected discovery of extensive gully networks during field surveys in the Crveni Potok catchment near Niš, Serbia—features that were completely invisible in available satellite imagery due to forest cover (Figure 1). The primary objectives of this study are to develop a reliable workflow for processing UAV LiDAR data to identify gully features beneath vegetation, to evaluate the effectiveness of topographic openness as a morphometric parameter for gully delineation, and to compare the automated extraction results with previously documented gullies from detailed terrestrial photogrammetric studies (Đokić et al., 2023; Manić et al., 2022).

2. Study area

The study was conducted in the Crveni Potok catchment, a forested tributary of the Malčanska River located in the border area of the Carpatho-Balkanides mountainous system in Eastern Serbia, covering approximately 8 km² and is elongated in the meridian direction, with elevation ranging from 284 m at the confluence with the Malčanska River to 729 m at the northern watershed divide (Manić et al., 2022).

The geology of the catchment is characterized by red Permian sandstone, conglomerate, and siltstone, which are highly susceptible to mechanical disintegration and water erosion. The soils in the catchment are primarily Haplic Cambisol (Eutric) formed on red sandstone, characterized as loamy, well-drained, medium-deep to deep, and erosion-prone. These parent materials and soil, combined with relatively steep slopes (often exceeding 20° in the northern parts), create conditions favorable for gully development (Figure 2) (Manić et al., 2022).

The climate is temperate continental with average annual precipitation ranging from 632 mm in the lower parts to 861 mm in the highest parts of the catchment. The largest precipitation occurs during late spring (May-June) and late autumn, with occasional high-intensity events that trigger torrential flows and accelerated erosion. Temperature rises in early spring often lead to rapid snow cover melting, which can coincide with rainfall and intensify water erosion processes (Manić et al., 2022).

Vegetation cover in the northern, higher-elevation areas of the catchment—which are the focus of this study—consists of forest and transitional woodland/shrub. The deciduous forest is dominated by Balkan sessile oak (Quercus delechampii), with other species including hornbeam (Carpinus), hawthorn (Crataegus), and hazel (Corylus). A small area at the northeast is covered by planted Scots pine (Pinus sylvestris). Full-strength old forest is rare in this area due to historical unplanned deforestation, with much of the current forest consisting of degraded stands with sparse canopy cover (Manić et al., 2022).

The catchment is characterized by intense surface water erosion, manifested primarily through gully erosion. Previous studies using terrestrial photogrammetry and nuclear techniques (^{137}Cs) have documented extensive gully networks in this area, with gullies ranging from a few tens of centimeters to several meters in depth (up to 8 m), and lengths from a few meters to several hundred meters (Manić et al., 2022; Đokić et al., 2023). These studies provided detailed morphometric characterization of individual gullies using 360-degree camera terrestrial photogrammetry and quantified soil erosion rates, establishing the Crveni Potok catchment as a well-documented reference area for gully erosion research.

Figure 2. *Field photograph of a gully within the Crveni Potok catchment.*

3. Materials and Methods

3.1. UAV LiDAR Data Acquisition

High-resolution topographic data were acquired using a Hesai XT32M2X LiDAR sensor mounted on a DJI M300 RTK drone. An Emlid RS3 Global Navigation Satellite System (GNSS) base station was used for log acquisition and post-processed kinematic (PPK) correction of the flight paths. This setup ensured centimeter-level accuracy during the acquisition process. Each individual scan produced approximately 70–80 GB of compressed raw data. Flight missions were planned to ensure adequate point density and coverage of the study area. The LiDAR survey was conducted under dense canopy (leaf-on) conditions, with well-developed and thick foliage. Key acquisition parameters included a flight altitude of 90 meters above ground level, a flight speed of 6 m/s, and a side overlap of 55%.

3.2. Point Cloud Processing

Raw LiDAR point clouds underwent several preprocessing steps to prepare the data for analysis. First, UAV trajectory data were processed using PCMasterProGL v1.7 software, which integrated GNSS and Inertial measurement unit (IMU) measurements to generate PPK-corrected flight paths, raw LiDAR scan files, and, where applicable, RGB colorization. These were converted into preliminary point clouds in LAS format. During this process, PCMasterProGL applied boresight corrections to eliminate systematic sensor errors and ensure accurate georeferencing, positioning, and orientation of each laser pulse. The resulting point clouds and flight trajectories were then imported into TerraScan v025.003 software. This comprised trajectory splitting to divide long flight lines into manageable segments, pass matching to align overlapping strips and minimize vertical misalignment, cut overlap to reduce redundant data in overlapped zones, smoothing and noise removal to filter outliers, and automated ground classification to separate ground points from vegetation and structural elements.

Following automated ground classification, the extracted ground points were subjected to manual inspection and editing to ensure data integrity and accuracy. This process involved a detailed visual review of the classified point clouds to identify misclassified features such as low vegetation or artificial structures that had been incorrectly labeled as ground. This ensured seamless integration of multiple flight missions, elimination of vertical offsets between surveys, and homogeneous point density across the catchment. The verified ground points were then exported in standard LAS

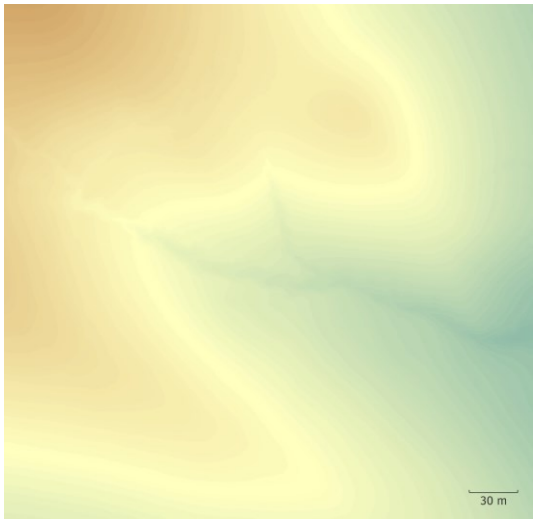

Figure 3. Bare-earth Digital Elevation Model (10 cm resolution) of the gully area derived from classified UAV LiDAR ground points.

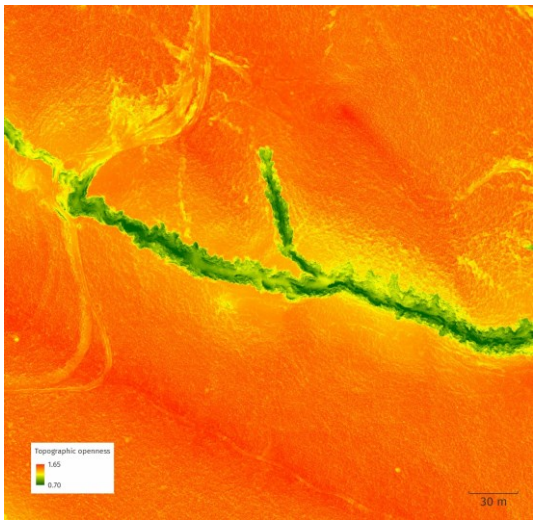

Figure 4. Positive topographic openness map.

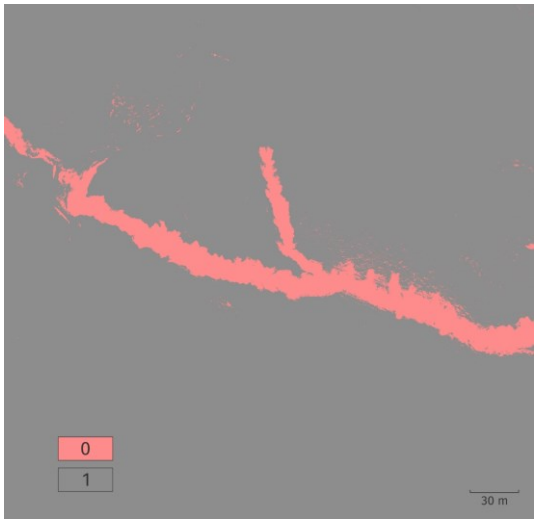

Figure 5. *Binary reclassification - class 0 openness values are below the gully threshold.*

format, providing a clean and spatially consistent input for subsequent DEM generation.

3.3. DEM Generation

Ground-classified point clouds, prepared in TerraScan, were exported in LAS format and imported into Agisoft Metashape Professional v2.1 for DEM generation. Metashape was selected for its robust capabilities in dense point cloud handling and raster surface modeling. Although widely recognized as leading photogrammetric software, Metashape also provides robust functionality for handling externally generated point clouds, making it suitable for producing high-resolution DEMs from UAV LiDAR datasets. A bare-earth Digital Elevation Model was then generated from the ground-classified points at a spatial resolution of 10 cm, providing the high level of detail necessary for gully detection (Figure 3). This resolution captures detailed gully morphology while maintaining manageable file sizes for processing.

3.4. Topographic Openness Computation

Positive topographic openness was calculated following the method of Yokoyama et al. (2002), Anders et al. (2009) and Doneus (2013). Topographic openness quantifies the angular relationship between a point and its surrounding terrain, providing a scale-independent measure of landform convexity and concavity (Figure 4).

For each cell in the DEM, zenith angles to the horizon were computed in multiple azimuthal directions. The positive openness at a given point is defined as the average of the minimum zenith angles measured in all directions. Concave features such as gullies exhibit low positive openness values, while convex features and ridges show high values.

The analysis was performed using the line tracing method, with a radial limit of 10,000 and an eight-sector configuration. The search radius was selected based on the expected width of gullies in the study area, ensuring that the analysis captured the full extent of gully morphology while remaining computationally feasible. Various DEM-based indices and hillshade methods have been employed for gully detection in different terrain conditions (Na et al., 2018; Omran et al., 2022).

3.5. Gully boundary Extraction

Gully boundaries were extracted through a series of raster processing operations. First, the topographic openness raster was reclassified into discrete landform classes. Threshold values were determined iteratively, and cells with openness below the critical threshold were classified as potential gully

areas (Figure 5). The resulting reclassified raster was then converted to vector polygons, producing preliminary gully boundaries that required further refinement (Figure 6). These vector polygons were subsequently simplified using the Douglas–Peucker algorithm to remove excessive detail while preserving essential morphological characteristics. Finally, isolated polygons smaller than 15 m² were removed to eliminate noise and retain only significant gully features (Figure 7).

The semi-automated extraction process was iteratively refined by comparing preliminary results with field observations and high-resolution imagery. Similar semi-automated approaches have been successfully employed in other gully mapping studies (Walker et al., 2024; Zhao et al., 2023).

3.6. Comparison with Terrestrial Photogrammetric Data

To evaluate the accuracy of the UAV LiDAR-based gully extraction, results were compared with previously published detailed gully mapping from the same catchment. Đokić et al. (2023) conducted comprehensive morphometric characterization of gullies in the Crveni Potok catchment using 360-degree camera terrestrial photogrammetry combined with nuclear techniques (^{137}Cs) for soil erosion quantification. Their study documented three major gullies (designated as Gullies A, B, and C) with high-resolution digital elevation models at 6-7 mm spatial resolution.

For this comparison, we selected Gully C from the Đokić et al. (2023) study, which represents a typical dendritic-type gully in the catchment. The portion of this gully documented in the previous study using 360-degree camera terrestrial photogrammetry is approximately 125 meters long, though the complete gully system extends considerably beyond this surveyed section. The 360-degree camera survey was limited to the accessible, traversable portion of the gully, as dense forest canopy and poor GNSS signal reception made georeferencing challenging in the upper reaches. The documented section has depths ranging from 0.4 to 3.5 meters and widths varying between 3.5 and 9 meters. The terrestrial photogrammetric model was generated from 518 aligned 360-degree images with a reprojection error of 5.07 pixels, resulting in a dense point cloud of over 92 million points and a final DEM resolution of 6.79 mm after ground point classification (Đokić et al., 2023). In contrast, the UAV LiDAR survey successfully captured the entire gully extent, including areas that were inaccessible or difficult to georeference with terrestrial methods.

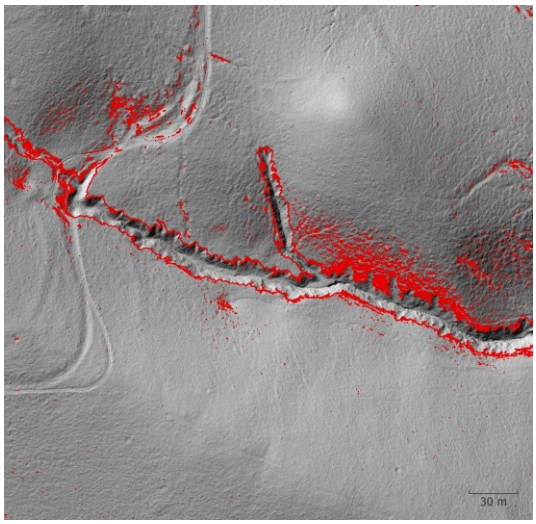

Figure 6. *Vectorized gully polygons (red).*

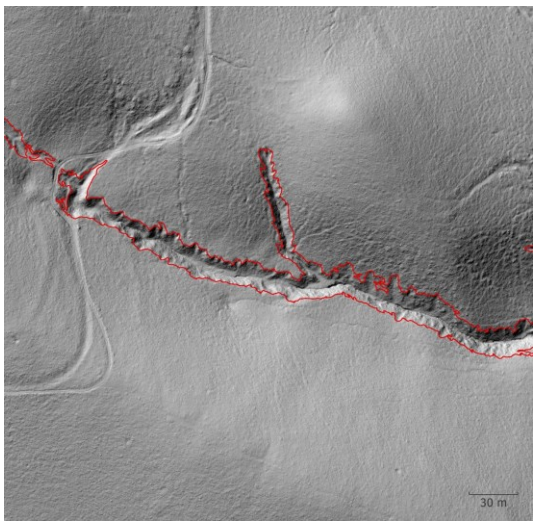

Figure 7. *Generalized gully boundary (red outline) after Douglas–Peucker simplification and small-polygon removal.*

The comparison methodology comprised three steps. First, the UAV LiDAR-derived gully boundaries were co-registered with the terrestrial photogrammetric DEM from Đokić et al. (2023) using common reference points. Gully C from their study was then compared with the automatically detected gully extracted from the UAV LiDAR-derived DEM using topographic openness analysis. Finally, a quantitative comparison of gully extent was performed.

3.7. Polygon Similarity and Boundary Accuracy Assessment

Spatial agreement between automatically extracted gully boundaries and the photogrammetric reference delineation was quantified using the polygon shape similarity framework proposed by Ďuračiová (2023). This framework integrates set-based overlap measures, geometric component

similarities, boundary distance metrics, and an aggregated shape similarity index (ASI), providing a multi-faceted evaluation of spatial correspondence. The concept of spatial similarity, discussed extensively across geometry, computer science, and geography (Yan and Li, 2015), is here expressed as a value between 0 (no spatial overlap) and 1 (identical spatial objects), following the formulation of Yan (2010).

Global spatial coincidence between polygons A (LiDAR-derived) and B (photogrammetric reference) was quantified using the Jaccard/Tanimoto index (Intersection over Union, IoU), defined as:

$$sim_J = \frac{| A \cap B |}{| A \cup B |}$$

As a complementary measure, the Dice coefficient was computed as:

$$sim_{DICE} = \frac{2 | A \cap B |}{| A | + | \cup B |}$$

Both indices provide normalized measures of areal agreement and are particularly sensitive to overall spatial coincidence between mapped features (Đuračiová, 2017; Tanimoto, 1958).

To account for structural differences beyond area overlap, component-level similarities were computed for polygon area, perimeter, and vertex count following the proportional-difference formulation of Đuračiová (2023):

$$sim_A = 1 - \frac{| Area_A - Area_B |}{max\ (Area_A, Area_B)}$$

$$sim_P = 1 - \frac{| Perimeter_A - Perimeter_B |}{max\ (Perimeter_A, Perimeter_B)}$$

$$sim_V = 1 - \frac{| Vertices_A - Vertices_B |}{max\ (Vertices_A, Vertices_B)}$$

Each term ranges from 0 (complete dissimilarity) to 1 (perfect agreement).

Positional accuracy of gully outlines was evaluated through boundary-based distance measures. The Hausdorff distance:

$$d_H(x,y) = max\left(sup_{X\in x} inf_{Y\in y} d(X,Y) sup_{Y\in y} inf_{X\in x} d(X,Y)\right)$$

quantifies the maximum deviation between polygon boundaries, while the Fréchet distance:

$$d_F(x,y) = inf_h sup_t |x(t) - y[h(t)]|$$

captures sequential geometric discrepancies along boundary trajectories. Both distances were normalized into similarity measures using a predefined tolerance threshold d_max:

$$sim_H = 1 - min\left(\frac{d_H}{d_{max}}, 1\right), sim_F = 1 - min\left(\frac{d_F}{d_{max}}, 1\right)$$

as proposed by Đuračiová (2023). Additionally, a boundary distance profile was generated by sampling points along the extracted gully boundary at regular intervals and computing the shortest Euclidean distance to the reference boundary, providing a continuous assessment of local spatial deviations along the entire feature perimeter.

Overall polygon similarity was summarized using the aggregated shape similarity index:

$$ASI = min\left(max(sim_H, sim_F, IoU), min(sim_A, sim_P, sim_V)\right)$$

This formulation ensures that both positional accuracy and geometric consistency jointly constrain the final similarity score (Đuračiová, 2023).

4. Results

The UAV LiDAR survey successfully acquired comprehensive coverage of the study area with an average point density of 1125.9 points/m². Ground point density after classification averaged 39.75 points/m², with higher densities in open areas and lower densities in densely forested zones.

The semi-automated extraction methodology successfully identified gully features within a 50-hectare test area of the catchment, with gullies covering a total mapped area of 3.2 hectares (Figure 8).

The automatically extracted gully polygon (A) exhibited excellent areal correspondence with the photogrammetric reference delineation (B). The Jaccard/Tanimoto index (IoU) reached 0.901, and the Dice coefficient attained 0.948, indicating near-complete spatial overlap. The intersection area amounted to 1,326 m², representing 97.3% of the LiDAR-derived polygon area (1,363 m²) and 92.4% of the photogrammetric reference area (1,434 m²). The total gully area derived from the LiDAR workflow was 4.9% smaller than the photogrammetric reference (1,363 m² vs. 1,434 m²).

Geometric component similarities revealed strong agreement in polygon area (sim_A = 0.95) and perimeter length (sim_P = 0.89), confirming that the extracted gully preserves both surface extent and boundary complexity. In contrast, vertex-based similarity was substantially lower (sim_V = 0.23), reflecting pronounced differences in boundary segmentation density between the automated extraction (2,238 vertices) and the manually digitized reference polygon (520 vertices).

Boundary distance analysis confirmed high positional accuracy. The mean boundary deviation was 0.47 m, with a median of 0.28 m, indicating predominantly sub-meter discrepancies. The 90th and 95th percentile errors remained below 1.32 m and 1.60 m, respectively, and the maximum deviation did not exceed 2.30 m. Approximately 67% of boundary points fell within 0.5 m of the reference boundary, 86% within 1 m, and nearly 98% within 2 m.

The Hausdorff distance between the two boundaries was 3.22 m, yielding a normalized Hausdorff similarity of sim_H = 0.36. The aggregated shape similarity index (ASI) attained a value of 0.23, constrained primarily by the low vertex similarity. Table 1 summarizes all computed similarity metrics.

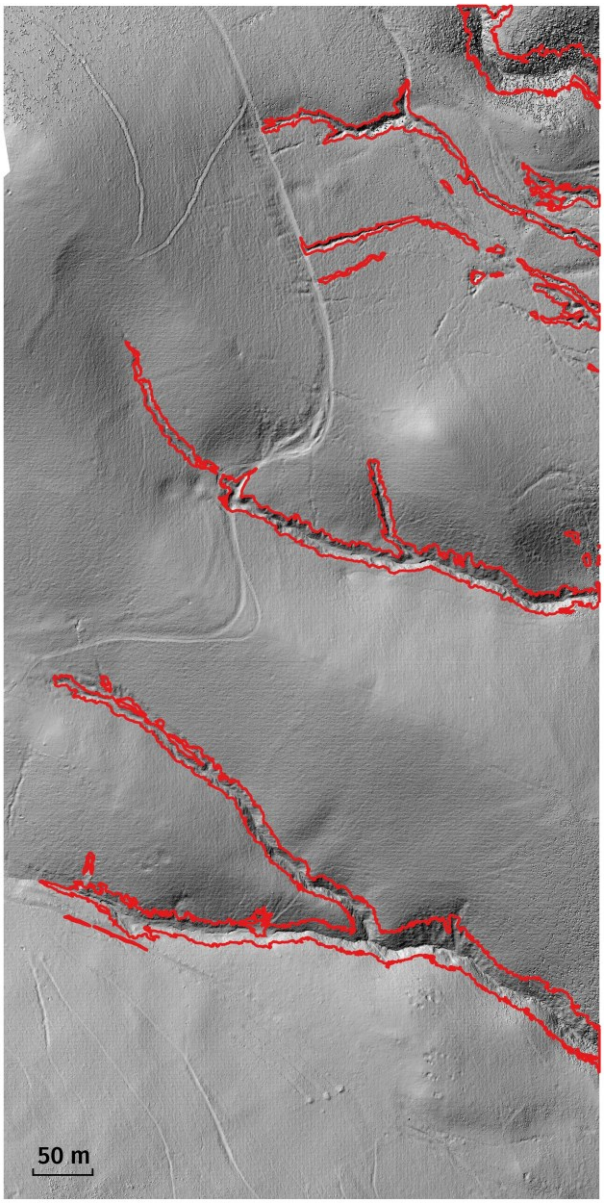

Figure 8. Semi-automatically detected gully boundaries overlaid on the UAV LiDAR-derived DEM of the catchment, showing a 50-hectare test area.

The boundary distance profile (Figure 9) reveals that deviations are generally concentrated below 0.5 m across most of the gully perimeter, with localized peaks of 1.5–2.3 m occurring at morphologically complex segments. The spatial overlay map (Figure 10) shows excellent correspondence between the two polygon boundaries along the main trunk of the gully, with the largest discrepancies confined to branching areas and the most sinuous portions of the boundary.

Table 1. Summary of polygon similarity and boundary accuracy metrics for Gully C. Polygon A = UAV LiDAR-derived boundary; Polygon B = 360-degree camera photogrammetric reference (Đokić et al., 2023).

Category	Metric	Value
Area-based metrics	Area A (m²)	1362.98
	Area B (m²)	1434.05
	Intersection area (m²)	1325.59
	Union area (m²)	1471.44
	Jaccard/Tanimoto index (sim_J)	0.901
	Dice coefficient	0.948
	Overlap relative to A (%)	97.26
	Overlap relative to B (%)	92.44
Shape complexity	Perimeter A (m)	367.52
	Perimeter B (m)	412.33
	Vertices A (n)	2238
	Vertices B (n)	520
Similarity indices	Area similarity (sim_A)	0.950
	Perimeter similarity (sim_P)	0.891
	Vertex similarity (sim_V)	0.232
	Adjusted Shape Index (ASI)	0.232
Distance-based metrics	Hausdorff distance (m)	3.215
	Normalized Hausdorff similarity (sim_H)	0.357
	Fréchet distance (m)	67.216
Profile distance statistics	Mean distance (m)	0.469
	Median distance (m)	0.279
	90th percentile (m)	1.317
	95th percentile (m)	1.599
	Minimum distance (m)	~0.000
	Maximum distance (m)	2.301
Threshold agreement	≤ 0.5 m (%)	67.47
	≤ 1.0 m (%)	85.54
	≤ 2.0 m (%)	97.59

5. Discussion

5.1. Effectiveness of UAV LiDAR for Gully Detection in Forested Terrain

This study demonstrates that UAV LiDAR technology provides a reliable and efficient means of detecting and mapping gullies in forested terrain where conventional remote sensing approaches fail. The ability of LiDAR to penetrate vegetation canopy proved essential for identifying gullies that were invisible in available satellite imagery.

The high point density achieved by UAV LiDAR (39.75 points/m²) enabled generation of a 10 cm resolution DEM, providing unprecedented detail for characterizing gully morphology. This level of detail is critical for accurate erosion assessment and exceeds what is typically achievable with airborne LiDAR or satellite-based techniques. The flexibility of UAV platforms also allowed data acquisition under optimal conditions and at lower cost than traditional aircraft-based LiDAR surveys.

However, vegetation density did influence data quality. While sufficient ground returns were obtained across most of the study area, very dense forest canopy reduced ground point density and introduced some uncertainty in gully delineation. This limitation could be partially addressed through acquiring data during leaf-off conditions for deciduous forests and from multiple scan directions. Similar challenges in dense vegetation have been reported in other LiDAR-based erosion studies (Kropáček et al., 2016).

While terrestrial photogrammetry can achieve millimeter-scale resolution, it faces significant practical limitations in forested terrain. The Đokić et al. 2023 encountered difficulties with georeferencing due to dense forest canopy obscuring GNSS signals, and was limited to surveying only the accessible, traversable portions of gullies. In contrast, UAV LiDAR provided consistent coverage across the entire study area, including inaccessible gully sections, with reliable georeferencing through PPK correction. Furthermore, the automated delineation methodology applied to the LiDAR data eliminates the subjectivity inherent in manual boundary digitization, providing a more objective and reproducible approach to gully mapping. The close agreement in gully area (4.9% difference) and high spatial overlap (92–97%) between the two methods validates the UAV LiDAR approach while demonstrating its advantages in spatial coverage, georeferencing accuracy, and methodological objectivity.

5.2. Topographic Openness as a Gully Detection Parameter

Positive topographic openness proved to be an effective morphometric parameter for highlighting gully features in the high-resolution DEM. The method successfully distinguished concave gully landforms from surrounding terrain without requiring complex multi-parameter analysis or machine learning approaches.

The scale-independent nature of topographic openness was particularly advantageous given the range of gully sizes in the study area. Unlike slope-based or curvature-based metrics that may require different parameter settings for features of different scales, openness calculations with appropriate search radius captured both small incipient gullies and large established features. This characteristic makes the method more robust and transferable to other study areas. Selection of the search radius parameter requires consideration of expected gully dimensions and terrain characteristics. Future applications should conduct preliminary analy-

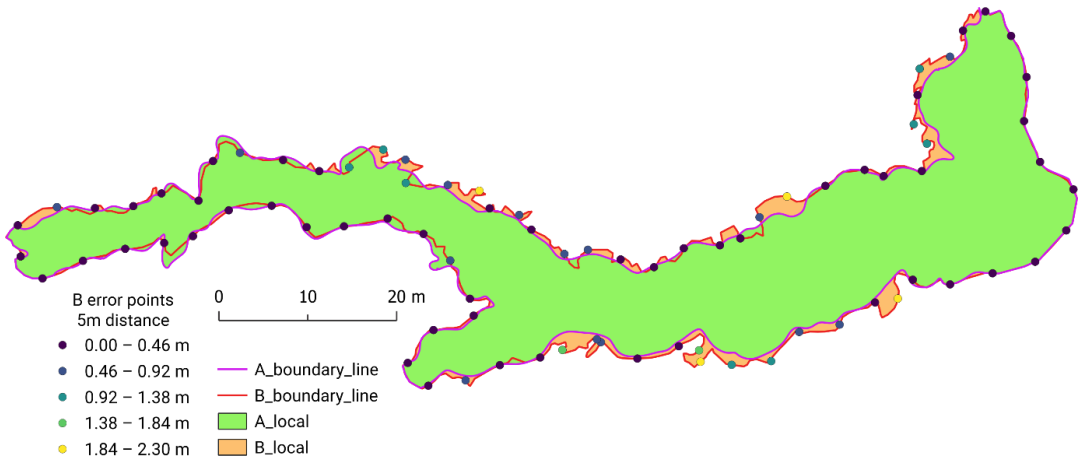

Figure 9. *Spatial overlay of the LiDAR-derived gully polygon (A, magenta boundary) and the photogrammetric reference polygon (B, red boundary) for Gully C. Green fill indicates the area of intersection; orange patches show areas of non-overlap. Colored points along the boundary are sampled error locations classified by distance magnitude.*

sis to optimize this parameter for local conditions. Alternative DEM-based approaches for gully detection include slope-area thresholds (Walker et al., 2024), bidirectional hillshade methods (Na et al., 2018), and hydrological modeling (Zhao et al., 2023), each with specific advantages depending on terrain characteristics and data resolution.

5.3. Interpretation of Polygon Similarity Metrics

Larger boundary deviations (1.5–2.3 m) occurred locally at highly curved or morphologically complex gully sections, particularly at tributary junctions and near the headcut area where the photogrammetric survey coverage was incomplete (Figure 8). These peaks reflect terrain-induced uncertainties and differences in survey extent rather than systematic errors in the extraction algorithm.

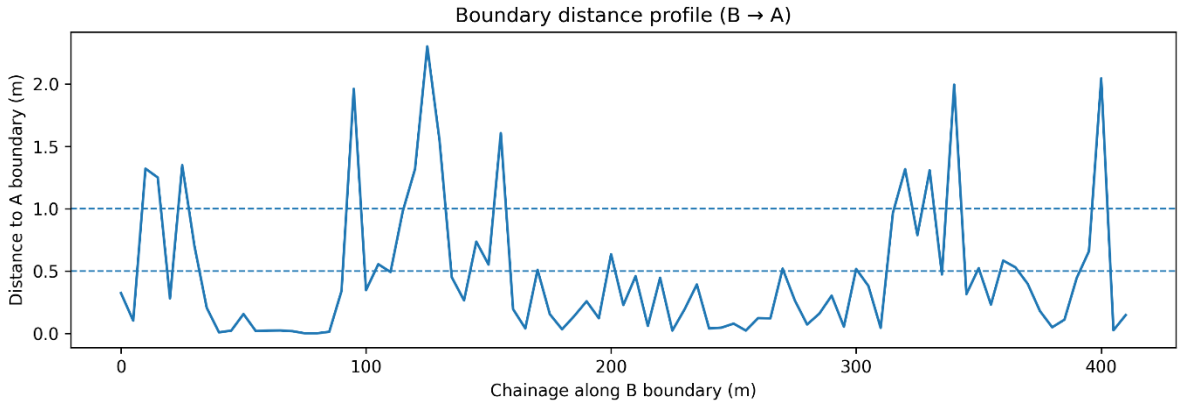

Figure 10. *Boundary distance profile along the extracted gully perimeter (polygon B → A). The horizontal axis represents chainage along the reference boundary; the vertical axis shows the shortest Euclidean distance to the LiDAR-derived boundary.*

The high IoU (0.901) and Dice coefficient (0.948) demonstrate near-complete areal correspondence between the LiDAR-derived gully boundary and the photogrammetric reference, with more than 92% of the reference area and 97% of the extracted area mutually coincident. Combined with predominantly sub-meter boundary deviations (mean 0.47 m, median 0.28 m), these results validate the spatial accuracy of the automated extraction workflow.

The notably low vertex similarity (sim_V = 0.23) and, consequently, the low aggregated ASI (0.23) require careful interpretation. The LiDAR-derived polygon contains 2,238 vertices—roughly four times more than the 520 vertices of the manually digitized reference. This disparity arises from fundamental differences in boundary generation: the automated raster-to-vector conversion followed by Douglas–Peucker simplification inherently produces denser vertex chains than manual digitization. As Ďuračiová (2023) emphasizes, vertex-based metrics are highly sensitive to generalization effects and algorithmic smoothing, and may therefore underestimate true similarity despite high positional correspondence. In the present case, the low ASI does not signal poor spatial performance but rather reflects the structural representation differences inherent to the two boundary-generation methods.

5.4. Sources of Error and Limitations

Two principal error sources affect the methodology. First, in areas where ground-point density falls below the level needed for reliable 10 cm interpolation, the resulting DEM may contain smoothing artifacts that blur fine-scale gully morphology. Such artifacts were most evident beneath the densest canopy patches and could lead to underestimation of gully width or depth at those locations.

Second, the spherical photogrammetric reference model itself carries positional uncertainty arising from limited GNSS reception under forest canopy and the geometrically challenging conditions inside deep, narrow gullies. These errors propagate into the derived terrain metrics and, consequently, into the reported spatial accuracy figures of the overlap comparison.

5. Conclusion

This study demonstrates that high-resolution UAV LiDAR enables accurate detection and mapping of gully erosion in forested terrain where conventional optical imagery fails. Positive topographic openness proved to be an effective scale-independent morphometric parameter, capable of highlighting gullies of varying sizes without iterative parameter tuning. The semi-automated extraction workflow

yielded gully boundaries that closely matched ultra-high-resolution terrestrial photogrammetric reference data. Overall, the proposed methodology offers a practical and transferable framework for catchment-scale erosion assessment, complementing detailed but spatially limited terrestrial studies.

Future research should extend the methodology to larger geographic areas to assess regional erosion patterns, while repeat surveys would enable quantification of gully expansion rates and sediment production over time. Integration of LiDAR-derived gully maps with hydrological and erosion process models represents a logical next step toward predictive capacity, alongside investigation of machine learning approaches for fully automated gully classification. The demonstrated success of UAV LiDAR for gully detection in challenging forested terrain, validated against independent ultra-high-resolution terrestrial data, opens new possibilities for comprehensive erosion monitoring and sustainable land management in similar environments worldwide.

Acknowledgements

This research was supported by the Science Fund of the Republic of Serbia (grant No. 7047), Development of erosion prediction tool for sustainable soil management—Predict-Er. This paper was also supported by the Ministry of Science, Technological Development and Innovation of the Republic of Serbia (contract 451-03-34/2026-03/200124).

ORCID iDs

Milan Đorđević https://orcid.org/0000-0001-8068-8906
Miloš Manić https://orcid.org/0000-0002-2452-5798

References

Anders, N. S. / Seijmonsbergen, A. C. / Bouten, W. (2009): Multi-Scale and Object-Oriented Image Analysis of High-Res LiDAR Data for Geomorphological Mapping in Alpine Mountains. Proceedings of Geomorphometry 2009. pdf at geomorphometry.org

Challis, K. (2006). Airborne laser altimetry in alluviated landscapes. Archaeological Prospection, 13(2), 103–127. https://doi.org/10.1002/arp.272

Doneus, M. (2013). Openness as visualization technique for interpretative mapping of airborne lidar derived digital terrain models. Remote Sensing, 5(12), 6427–6442. https://doi.org/10.3390/rs5126427

Đokić, M., Manić, M., Đorđević, M., Gocić, M., Cupić, A., Jović, M., Dragović, R., Gajić, B., Smičiklas, I., & Dragović, S. (2023). Remote sensing and nuclear techniques for high-resolution mapping and quantification of gully erosion in the highly erodible area of the Malčanska River Basin, Eastern Serbia. Environmental Research, 235, 116679. https://doi.org/10.1016/j.envres.2023.116679

Ďuračiová, R. (2023). An Aggregated Shape Similarity Index: A Case Study of Comparing the Footprints of OpenStreetMap and INSPIRE Buildings. ISPRS International Journal of Geo-Information, 12(12), 495. https://doi.org/10.3390/ijgi12120495

Ďuračiová, R., & Igondová, M. (2017). Integration of spatial data representing buildings by determining the degree of similarity. Czech Journal of Civil Engineering, 3, 29–35. https://doi.org/10.51704/cjce.2017.vol3.iss1.pp29-35

Hodgson, M.E., & Bresnahan, P. (2004). Accuracy of airborne lidar-derived elevation: Empirical assessment and error budget. Photogrammetric Engineering & Remote Sensing, 70(3), 331–339. https://doi.org/10.14358/PERS.70.3.331

Jaboyedoff, M., Oppikofer, T., Abellán, A., Derron, M.H., Loye, A., Metzger, R., & Pedrazzini, A. (2012). Use of LIDAR in landslide investigations: A review. Natural Hazards, 61(1), 5–28. https://doi.org/10.1007/s11069-010-9634-2

Kropáček, J., Schillaci, C., Salvini, R., & Märker, M. (2016). Assessment of gully erosion in the Upper Awash, Central Ethiopian Highlands based on a comparison of archived aerial photographs and very high resolution satellite images. Geografia Fisica e Dinamica Quaternaria, 39(2), 161–170. https://dx.doi.org/10.4461/GFDQ.2016.39.15

Liu, X. (2008). Airborne LiDAR for DEM generation: Some critical issues. Progress in Physical Geography, 32(1), 31–49. https://doi.org/10.1177/0309133308089496

Manić, M., Đorđević, M., Đokić, M., Dragović, R., Kićović, D., Đorđević, D., Jović, M., Smičiklas, I., & Dragović, S. (2022). Remote sensing and nuclear techniques for soil erosion research in forest areas: Case study of the Crveni Potok catchment. Frontiers in Environmental Science, 10, 897248. https://doi.org/10.3389/fenvs.2022.897248

Na, J., Yang, X., Dai, W., Li, M., Xiong, L., Zhu, R., & Tang, G. (2018). Bidirectional DEM relief shading method for extraction of gully shoulder line in loess tableland area. Physical Geography, 39(4), 368–386. https://doi.org/10.1080/02723646.2017.1410974

Omran, A., Schröder, D., Sommer, C., Hochschild, V., & Märker, M. (2022). A GIS-based simulation and visualization tool for the assessment of gully erosion processes. Journal of Spatial Science. https://doi.org/10.1080/14498596.2022.2133020

Poesen, J., Nachtergaele, J., Verstraeten, G., & Valentin, C. (2003). Gully erosion and environmental change: Importance and research needs. Catena, 50(2–4), 91–133. https://doi.org/10.1016/S0341-8162(02)00143-1

Tanimoto, T. (1958). An Elementary Mathematical Theory of Classification and Prediction (Tech. Rep.). IBM: New York, NY, USA.

Valentin, C., Poesen, J., & Li, Y. (2005). Gully erosion: Impacts, factors and control. Catena, 63(2–3), 132–153.

Vosselman, G., & Maas, H.G. (Eds.). (2010). Airborne and Terrestrial Laser Scanning. Whittles Publishing, Scotland, UK.

Walker, S.J., Wilkinson, S.N., & Hairsine, P.B. (2024). Advancing gully topographic threshold analysis using an automated algorithm and high-resolution topography. Catena, 239, 107897. https://doi.org/10.1016/j.catena.2024.107897

Yan, H. (2010). Fundamental theories of spatial similarity relations in multi-scale map spaces. Chinese Geographical Science, 20, 18–22. https://doi.org/10.1007/s11769-010-0018-z

Yan, H., & Li, J. (2015). Spatial Similarity Relations in Multi-Scale Map Spaces. Springer International Publishing, Cham, Switzerland, 188p. https://doi.org/10.1007/978-3-319-09743-5

Yokoyama, R., Shirasawa, M., & Pike, R.J. (2002). Visualizing topography by openness: A new application of image processing to digital elevation models. Photogrammetric Engineering & Remote Sensing, 68(3), 257–265.

Zhao, M., Qi, J., Ju, X., Zhang, Y., Wang, C., Xu, Y., & Sun, J. (2023). A novel gully network extraction method combining hydrological confluence process and surface morphology. Journal of Mountain Science, 20(9), 2536–2556. https://doi.org/10.1007/s11629-023-7933-9